

Tests des Standardmodells der Teilchenphysik

Spezialfach Kern-Teilchen-Astrophysik

Tests of the Standard Model of Particles

Spring Semester 2018

Lecture 1

Dr. Zinonas Zinonos
zinonos@mpp.mpg.de

Max-Planck-Institut für Physik, TUM

March 12, 2018

About

Tests of Standard Model I: <https://www.mpp.mpg.de/~zinonos/>

Tests of Standard Model II:

Main course

- ▶ Thursday, 14:00-16:00
- ▶ PH 2271, Seminarraum (5101.EG.271)

Tutorials

- ▶ Friday, 12:00-14:00
- ▶ C.3203, Tutorraum (5140.01.203)
- ▶ After consultation in the class

Overview

- Higgs boson properties
- Higgs boson decays
- Higgs search channels
- Higgs production mechanisms
- Hadron colliders and detectors
- Searching for the Higgs boson at hadron colliders

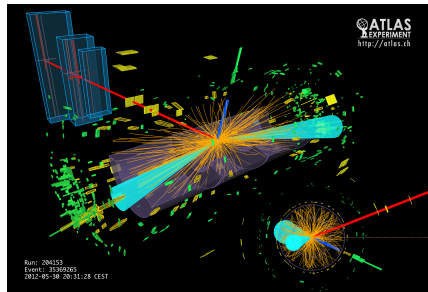


Figure 1: A Higgs to 2 τ candidate event in ATLAS.

Higgs boson properties

- ▶ The Standard Model Higgs boson H is a neutral scalar particle.
- ▶ The Higgs boson mass cannot be predicted by the Standard Model as λ of the Higgs potential is a *free* parameter

$$m_H = \sqrt{2\lambda}v \quad \text{with} \quad v = 246 \text{ GeV} \quad (1)$$

- ▶ The Higgs boson couples to all massive gauge bosons with a coupling strength proportional to $g_V m_V$ with $V = W, Z$.
- ▶ The Higgs boson couples to all fermions with a coupling strength proportional to the fermion mass,

$$\frac{g_f}{\sqrt{2}} = \frac{m_f}{v} \quad \text{Yukawa coupling} \quad (2)$$

- ▶ The Higgs Lagrangian of the fermion sector is

$$L_f = -m_f \bar{f}f - \frac{m_f}{v} \bar{f}f h \quad (3)$$

From which the Feynman rule for the interaction vertex with a fermion of mass m_F can be identified as

$$-i \frac{m_f}{v} \equiv -i \frac{m_f}{2m_W} g_W \quad (4)$$

The Higgs boson can therefore decay via $H \rightarrow \bar{f}f$ and $H \rightarrow VV$ for all kinematically allowed decay modes with $m_H > 2m_f$ and $m_H > 2m_V$, respectively .

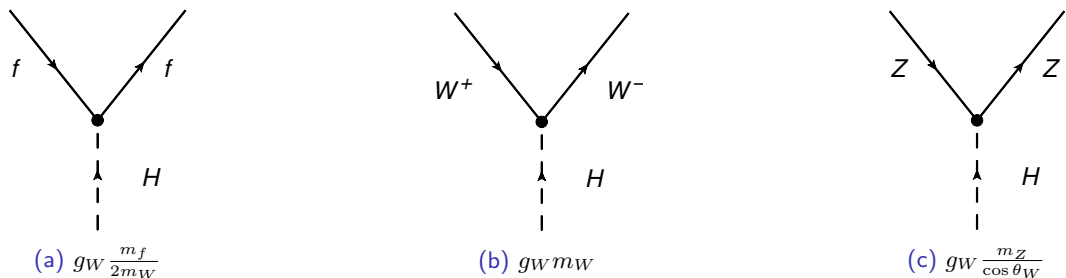


Figure 2: Feynman diagrams and coupling strengths for these lowest-order decay modes.

In each case, the Higgs boson coupling is proportional to the decay particle mass, determining thus the dominant processes through which it is produced and decays

The Higgs boson couples preferentially to the **most massive particles** that are kinematically accessible.

Higgs decay into fermions

Let us consider the Higgs boson mass m_h as a free parameter. The coupling of the Higgs boson h^0 to a fermion pair $\bar{f}f$, either leptons or quarks, can be described by the Lagrangian

$$\mathcal{L}_f = -\frac{1}{v}m_f h^0 \bar{f}f \quad (5)$$

and hence at tree level the matrix element is

$$i\mathcal{M} = -i\frac{1}{v}m_f \bar{u}^s(p)v^r(k) \quad (6)$$

Therefore, the $h^0 \rightarrow \bar{f}f$ involves a single Yukawa vertex only. To calculate the decay width we firstly need to find an expression of the squared matrix element of the decay process,

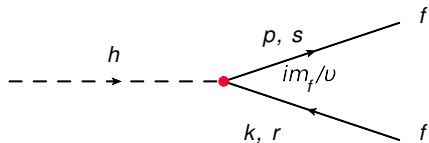


Figure 3: Higgs decay into charged fermions.

By calculating the squared amplitude and simply summing over the fermion spins

$$\langle |\mathcal{M}|^2 \rangle = \sum_{\text{spins}} (i\mathcal{M})(i\mathcal{M})^\dagger. \quad (7)$$

since the Higgs boson has only one polarization state, we find

$$\langle |\mathcal{M}|^2 \rangle = \frac{2m_f^2}{v^2} (m_h^2 - 4m_f^2) = 2\sqrt{2}G_F m_f^2 (m_h^2 - 4m_f^2) \quad (8)$$

since

$$\frac{G_F}{\sqrt{2}} = \frac{g^2}{8m_w^2} \quad \text{and} \quad m_W = \frac{1}{2}gv \quad (9)$$

The differential decay width for a two-body decay is given by

$$\frac{d\Gamma}{d\Omega} = \frac{1}{m_h} \langle |\mathcal{M}|^2 \rangle \frac{1}{32\pi^2} \frac{2|p_f|}{m_h} \quad (10)$$

Integrating over $d\Omega = d\phi d\cos\theta$ (and since there is no angular dependence, $\int d\Omega = 4\pi$), one obtains the partial decay width.

The decay width is therefore

$$\Gamma(h^0 \rightarrow \bar{f}f) = N_c^f \times \frac{G_F}{4\pi\sqrt{2}} m_h m_f^2 \left[1 - \left(\frac{2m_f}{m_h} \right)^2 \right]^{3/2}, \quad \text{where } N_c^f = \begin{cases} 1 & \text{for leptons} \\ 3 & \text{for quarks} \end{cases}. \quad (11)$$

The factor of $N_c = 3$ accounts for the three possible color of the $\bar{q}q$ pair.

Assuming $m_h \gg 2m_f$, the decay width can be approximated as

$$\Gamma(h^0 \rightarrow \bar{f}f) \simeq N_c^f \times \frac{m_h m_f^2}{8\pi v^2} \propto m_f^2 \quad \text{with } v = \frac{1}{\sqrt{\sqrt{2}G_F}} = 246 \text{ GeV} \quad (12)$$

→ Therefore, the Higgs boson decays dominantly into the heaviest fermions and width $\propto m_h$.
For example, a Higgs boson mass of 125 GeV, the partial decay width $\Gamma(H \rightarrow \bar{b}b)$ is $\mathcal{O}(2 \text{ MeV})$.

Note that, quark masses run with q^2 in a similar manner to the running of strong coupling α_s .

↪ Hence the quark masses appearing in Γ are the appropriate values at $q^2 = m_h^2$, for example

- ▶ $m_c(m_h^2) \approx 0.6 \text{ GeV}$
- ▶ $m_b(m_h^2) \approx 3.0 \text{ GeV}$

Higgs decay into gauge bosons

The Yukawa couplings of the Higgs bosons to the massive gauge bosons $V = W^\pm, Z^0$ are

$$\mathcal{L}_V = \frac{1}{v} \left(2M_W^2 h^0 W_\mu^+ W^{-\mu} + M_Z^2 h^0 Z_\mu^0 Z^{0\mu} \right) \quad (13)$$

and thus the amplitude for the $h^0 \rightarrow W^+ W^-$ process is

$$i\mathcal{M} = \frac{1}{2} v g^2 g^{\mu\nu} \epsilon_\mu^*(p, \lambda) \epsilon_\nu^*(k, \rho) . \quad (14)$$

We can show that in the on-shell approximation the decay width is

$$\Gamma(h^0 \rightarrow W^+ W^-) = \frac{G_F}{8\pi\sqrt{2}} m_h^3 (1 - 4\lambda_W)^{\frac{1}{2}} (1 - 4\lambda_W + 12\lambda_W^2) , \quad (15)$$

where $\lambda_W = (M_W/m_h)^2$.

Similarly, show that decay rate for the process $h^0 \rightarrow Z^0 Z^0$ is

$$\Gamma(h^0 \rightarrow Z^0 Z^0) = \frac{G_F}{16\pi\sqrt{2}} m_h^3 (1 - 4\lambda_Z)^{\frac{1}{2}} (1 - 4\lambda_Z + 12\lambda_Z^2) , \quad (16)$$

where $\lambda_Z = (M_Z/m_h)^2$.

The decay width grows like m_h^3 , i.e. is very large for $m_h \gg m_V$. For small m_h , one (two) V bosons can be off-shell, the width is

$$\Gamma = \frac{\Gamma_0}{\pi^2} \int_0^{m_h^2} \frac{dq_1^2 M_V \Gamma_V}{(q_1^2 - M_V^2)^2 + M_V^2 \Gamma_V^2} \int_0^{m_h^2 - q_1^2} \frac{dq_2^2 M_V \Gamma_V}{(q_2^2 - M_V^2)^2 + M_V^2 \Gamma_V^2} \quad (17)$$

with

$$\Gamma_0 = S_V \frac{m_h^3}{8\pi v^2} \Lambda^{1/2} \left(\Lambda - 12 \frac{q_1^2 q_2^2}{m_h^4} \right), \quad \Lambda = \left(1 - \frac{q_1^2}{m_h^2} - \frac{q_2^2}{m_h^2} \right)^2 - 4 \frac{q_1^2 q_2^2}{m_h^4}. \quad (18)$$

and $S_V = 1$ or 2 .

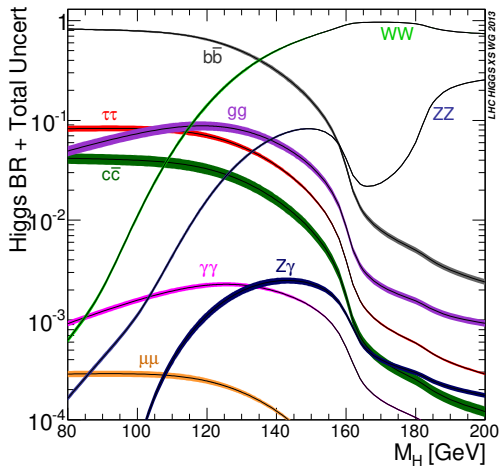
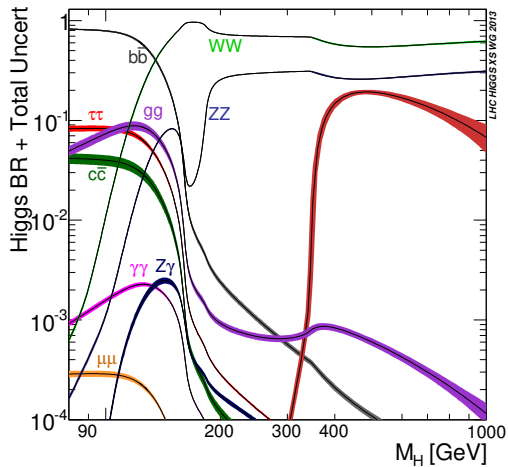


Figure 4: Standard Model Higgs boson decay branching ratios and total width.

↪ Despite the fact that $m_H < 2m_W$, the second largest branching ratio is for the decay $H \rightarrow W^*W$, where one of the W bosons is produced off-mass-shell with $q^2 < m_W^2$.

From the form of the W-boson propagator of

$$|\mathcal{M}|^2 \propto \frac{1}{[(q^2 - m_W^2)^2 + m_W^2 \Gamma_W^2]^2} \quad (19)$$

the presence of the off-shell W boson will tend to suppress the matrix element.

Nevertheless, the large coupling of the Higgs boson to the massive W boson, $g_W m_W$ yields to relatively large branching ratios.

Decay Mode	Branching Ratio
$b\bar{b}$	57.8%
W^*W	21.6%
$\tau^+\tau^-$	6.4%
gg	8.6%
$c\bar{c}$	2.9 %
Z^*Z	2.7%
$\gamma\gamma$	0.2%

Table 1: The predicted branching ratios of the Higgs boson for $m_H = 125$ GeV.

Higgs decay to massless particles

The Higgs boson also can decay to massless particles, such as $H \rightarrow gg$ and $H \rightarrow \gamma\gamma$, through loops of virtual top quarks and W bosons.

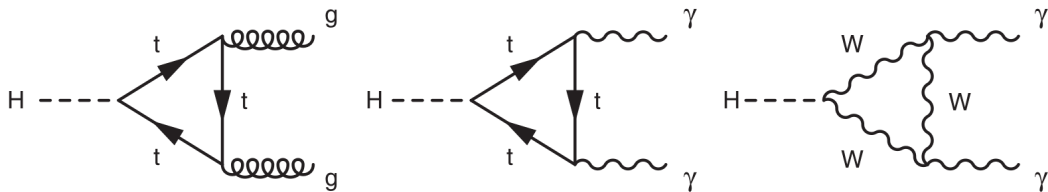


Figure 5: The Feynman diagrams for the decays $H \rightarrow gg$ and $H \rightarrow \gamma\gamma$.

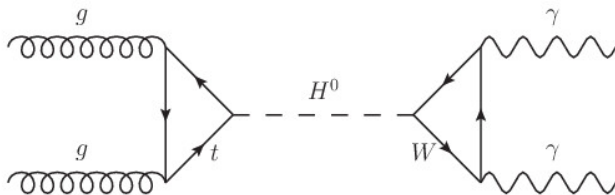
The masses of the particles in these loops are large and thus such decay modes can compete with the decays to fermions and the off-mass-shell gauge bosons.

Search channels

The most important Higgs boson decay modes that can be used in collider experiments in the mass region of the Higgs particle are:

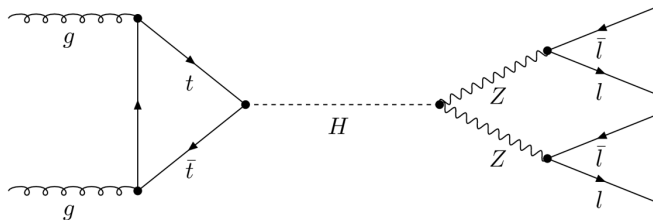
$H \rightarrow \gamma\gamma$

- ▶ Although the branching ratio of this channel is very low (BR 0.2 %), it provides the best sensitivity in the low mass region.
- ▶ A very good photon identification, robust against QCD multijets that might be possibly faking photons, as well as an excellent energy reconstruction are the key ingredients for the measurement in this channel.
- ▶ The diphoton invariant mass spectrum $m_{\gamma\gamma}$ is used as the discriminating variable.



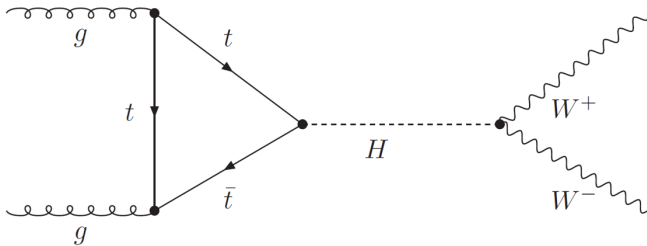
$H \rightarrow ZZ \rightarrow 4\ell$

- ▶ This is considered to be the "golden channel" since it would possess the cleanest signal in the intermediate Higgs boson mass range.
- ▶ However, the branching ratio below 150 GeV decreases rapidly and it is more difficult to use this channel also in the low mass range.
- ▶ The search is based on identifying two pairs of isolated leptons with same flavor (SF) and opposite electric charges (OS).
- ▶ The invariant mass of the four leptons' system is considered as the discriminant. A high efficiency of the lepton trigger (online data acquisition) and lepton identification as well as a very good energy resolution are required for the precise measurement in this decay mode.



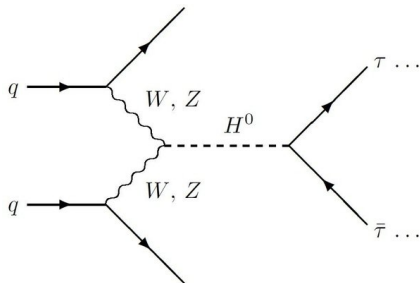
$H \rightarrow WW(\rightarrow 2l\nu)$

- ▶ The decay mode with two W bosons could potentially lead to the best sensitivity in the intermediate Higgs boson mass range and it could also contribute in the lowest Higgs boson mass range.
- ▶ The cleanest experimentally signature is formed by a pair of isolated leptons with opposite charges and large missing transverse energy due to the escaping neutrinos.
- ▶ The invariant mass cannot be reconstructed and therefore the transverse mass of the Higgs boson is used as the discriminant.



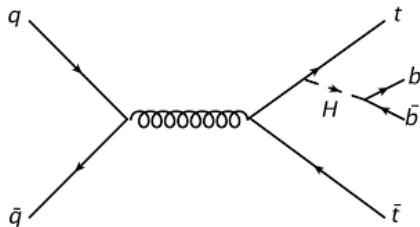
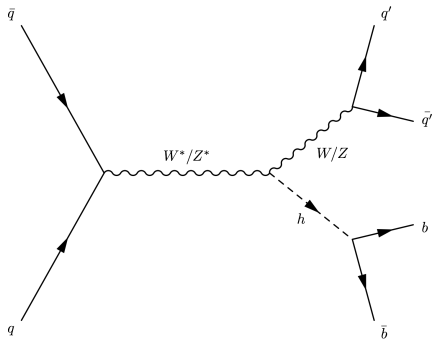
$H \rightarrow \tau\tau$

- ▶ The Higgs decay mode with a pair of τ leptons is measurable in the low mass region.
- ▶ The difficulty of the search in this channel comes from the hadronic τ decay which might appear in the final state as a jet can be easily misidentified as a real hadronic τ .
- ▶ Therefore the large multijet background must be carefully taken under control.
- ▶ If the mass of the Higgs boson then background $Z \rightarrow \tau\tau$ events become important.
- ▶ The invariant mass of the Higgs boson cannot be directly reconstructed due to neutrinos from the τ leptons' decays and thus complex mass reconstruction techniques must be deployed.

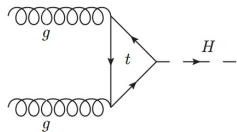


$H \rightarrow b\bar{b}$

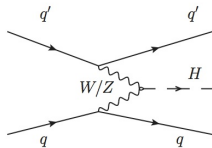
- ▶ This is the decay mode with the dominant branching ratio in the low mass region.
- ▶ However, it is very challenging to detect over the overwhelming QCD multijet background.
- ▶ It can be performed only in the associated production of the Higgs boson with electroweak bosons (ZH , WH) or with a top quark pair ($t\bar{t}H$).



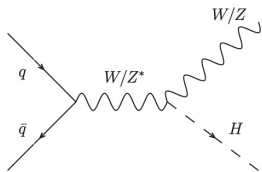
Higgs production mechanisms



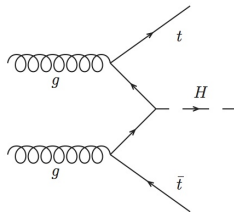
a)



b)



c)



d)

Main production mechanisms at hadron colliders:

- (a) gluon-gluon fusion (ggH),
- (b) vector-boson fusion (VBF),
- (c) VH association or *Higgsstrahlung*,
and
- (d) $t\bar{t}H$ association production.

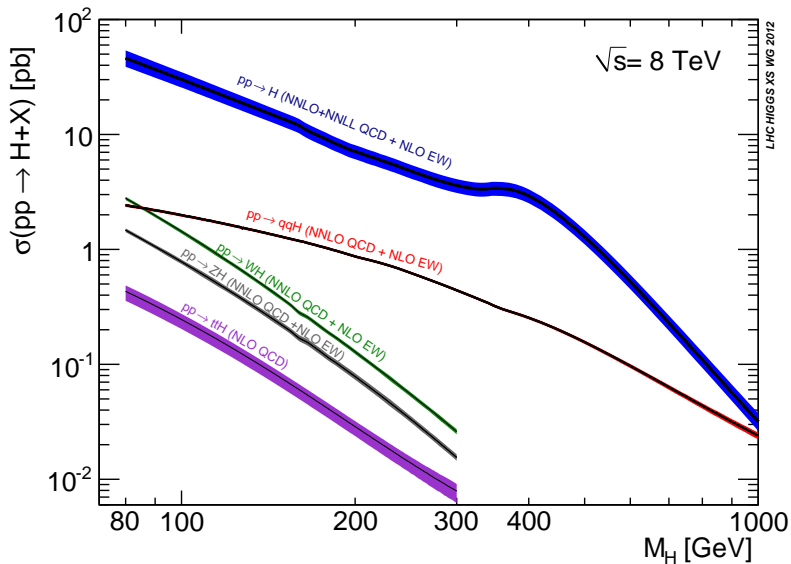


Figure 6: Standard Model Higgs boson production cross sections at $\sqrt{s} = 8$ TeV.

Main tools for Higgs hunting

To establish a discovery of the Higgs mechanism we need to

- ▶ discover the Higgs boson directly at a high-energy collisions
 - ▶ Hadron collider with high \sqrt{s} and high collision rate
 - ▶ Excellent detectors with high particle identification and four-momentum reconstruction
- ▶ measure the couplings g_{hXX}

$$\text{fermions: } g_{hff} = \sqrt{2} \frac{m_f}{v} \quad (20)$$

$$\text{gauge bosons: } g_{hVV} = 2 \frac{m_V}{v} \quad (21)$$

- ▶ reconstruct the Higgs mass m_h and its potential

The Higgs sector and the properties of the Higgs particle (lifetime, decay branching ratios, cross sections) are fixed in terms of the Higgs boson mass m_h :

- ▶ Express Higgs potential in terms of $(\mu, \lambda) \propto (v^2, m_h)$

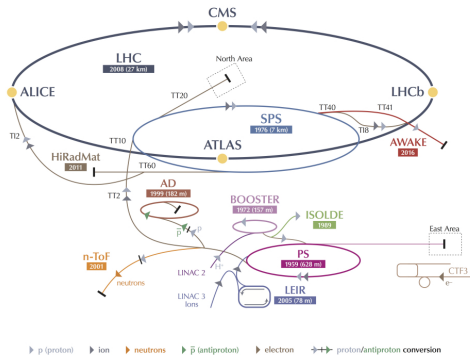
with

$$v^2 = \frac{1}{\sqrt{G_F}} = 246 \text{ GeV} \quad (22)$$

The leading-edge experimental program, energy-frontier experiment nowadays is the **Large Hadron Collider at CERN, Geneva.**

Large Hadron Collider

CERN's Accelerator Complex



LHC Large Hadron Collider SPS Super Proton Synchrotron PS Proton Synchrotron

AD Antiproton Decelerator CTF3 Clic Test Facility AWAKE Advanced WAKEfield Experiment ISOLDE Isotope Separator OnLine DEvice

LEIR Low Energy Ion Ring LINAC LINear ACcelerator n-ToF Neutrons Time Of Flight HiRadMat High-Radiation to Materials

© CERN 2013

Located at CERN, Geneva.

Circumference 27 km.

Most powerful collider complex in world and largest cryogenic facility ever built by mankind.

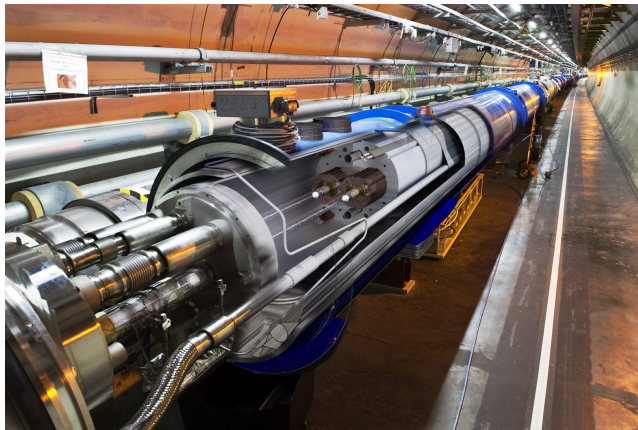
Collides bunches of protons up to $\sqrt{s} = 14$ TeV.

$$\int dt L = 10 - 100 \text{ fb}^{-1} / \text{year}$$

Operating since April 2017.



At the LHC the dipole magnets are superconducting electromagnets and designed to provide the very high field of 8.3 T over their length.



The LHC dipoles use niobium-titanium (NbTi) cables, which become superconducting below a temperature of 10 K ($-263.2\text{ }^{\circ}\text{C}$). In fact, the LHC will operate at 1.9 K ($-271.3\text{ }^{\circ}\text{C}$), which is even lower than the temperature of outer space (2.7 K or $-270.5\text{ }^{\circ}\text{C}$).

How many collisions per second take place at the LHC?

In the LHC, under nominal operating conditions, each proton beam has 2808 bunches, with each bunch containing about 10^{11} protons.

At full luminosity the LHC uses a bunch spacing of 25 ns (or 7.5 m). The bunch spacing of 25 ns corresponds to a frequency of 40 MHz, which implies that bunches should pass each of the collision points in the LHC 40 million times a second.

The particles are so tiny that the chance of any two colliding is very small. When the bunches cross, there are on average 40 collisions between 200 billion particles.

So, the LHC generates about 1.5 billion particle collisions per second.

Luminosity

In scattering theory and accelerator physics, luminosity (L) is the ratio of the number of events detected (N) in a certain time period (t) to the interaction cross-section (σ),

$$L = \frac{1}{\sigma} \frac{dN}{dt} \quad (23)$$

L has the dimensions of events per time per area, and is usually expressed in units of $\text{cm}^{-2}\text{s}^{-1}$.

In practice, **instantaneous luminosity** L is dependent on the particle beam parameters. Colliders which employ two bunches containing n_1 and n_2 particles collide head-on with frequency f_{coll} , a basic expression for the luminosity is

$$L = f_{\text{coll}} \frac{n_1 n_2}{4\pi \sigma_x \sigma_y} \quad (24)$$

where σ_x and σ_y characterize the rms transverse beam sizes in the horizontal (bend) and vertical directions.

A related quantity is **integrated luminosity** (L_{int}), which is the integral of the luminosity with respect to time:

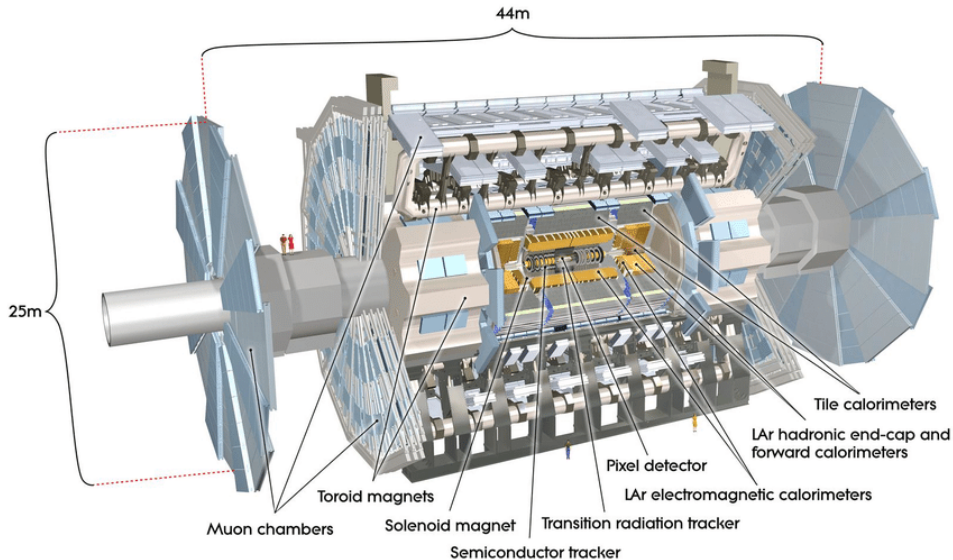
$$L_{\text{int}} = \int L dt. \quad (25)$$

The luminosity and integrated luminosity are useful values to characterize the performance of a particle accelerator.

In particular, all collider experiments aim to maximize their integrated luminosities, as the higher the integrated luminosity, the more data is available to analyze.

The design luminosity of the LHC is $10^{34} \text{cm}^{-2} \text{Hz}$, which was first reached in June 2016. By 2017 twice the nominal value was achieved.

A Toroidal LHC Apparatus Detector



ATLAS detector:

- ▶ multipurpose detector to search for the Higgs boson and new physics.
- ▶ 4π , hermetic detector
- ▶ cylindrical structure

The four major components of the ATLAS detector are:

- ▶ the Inner Detector;
- ▶ the Calorimeter;
- ▶ the Muon Spectrometer; and
- ▶ the Magnet System.

Integrated with the detector components are:

- ▶ the Trigger and Data Acquisition System, a specialized multi-level computing system, which selects physics events with distinguishing characteristics; and
- ▶ the Computing System, which develops and improves computing software used to store, process and analyze vast amounts of collision data at 130 computing centres worldwide.

ATLAS inside [view](#)

Coordinate system

The nominal interaction point is defined as the origin of the coordinate system, while the beam direction defines the z -axis and the x - y plane is transverse to the beam direction.

The positive x -axis is defined as pointing from the interaction point to the center of the LHC ring and the positive y -axis is defined as pointing upwards.

At the ultra-relativistic limit, $E \gg m$, particles' position is defined by the (η, ϕ) coordinate variables.

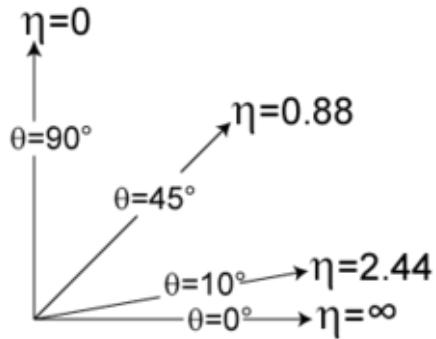
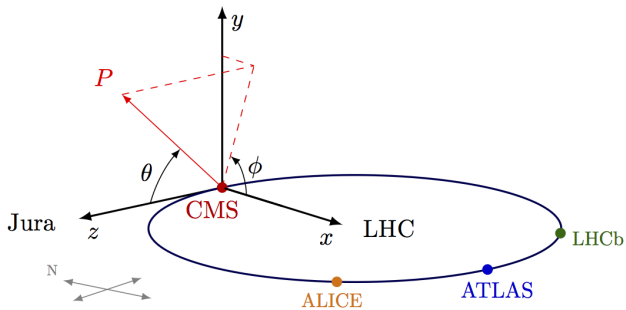
The azimuthal angle ϕ is measured around the beam axis and the polar angle θ is the angle from the beam axis.

The pseudorapidity is defined as

$$\eta = -\ln \tan \frac{\theta}{2} \quad (26)$$

The transverse momentum p_T and the transverse energy E_T are defined in the x - y plane. The distance ΔR in the η - ϕ space is defined as

$$\Delta R = \sqrt{(\Delta\eta)^2 + (\Delta\phi)^2} \quad (27)$$



Inner detector

The inner detector is the first part of ATLAS to see the decay products of the collisions, so it is very compact and highly sensitive.

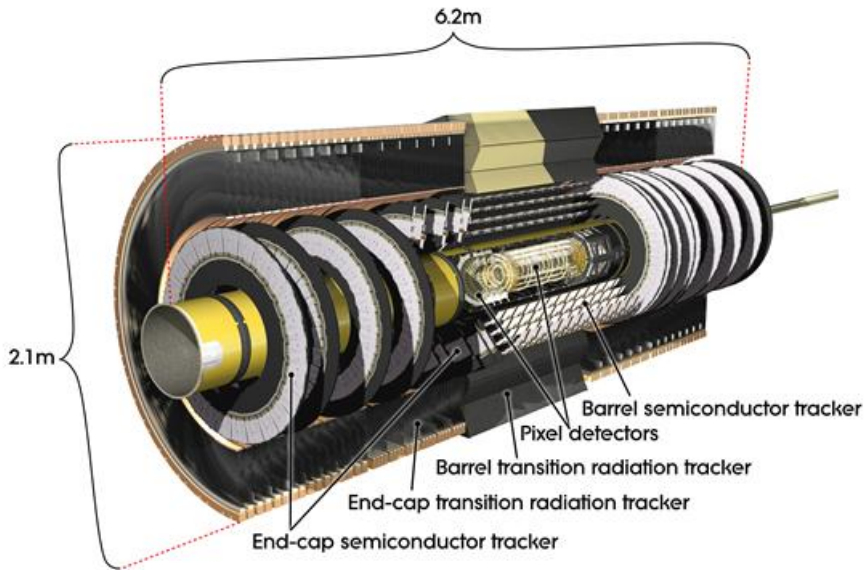
It consists of three different systems of sensors all immersed in a 2 T magnetic solenoidal field parallel to the beam axis.

The Inner Detector measures the direction, momentum, and charge of electrically-charged particles produced in each proton-proton collision.

The main components of the Inner Detector are:

- ▶ Pixel Detector,
- ▶ Semiconductor Tracker (SCT), and
- ▶ Transition Radiation Tracker (TRT).

The tracking system has an expected resolution of $\sigma_{p_T}/p_T = 0.05\% p_T \oplus 1\%$ with p_T in GeV in the whole pseudorapidity coverage of $|\eta| < 2.5$.



The **precision pixel** and **silicon microstrip (SCT)** trackers with a very fine segmentation cover the pseudorapidity range up to $|\eta| < 2.5$.

The precision tracking detectors are arranged on concentric cylinders around the beam axis while in the end-caps they are located on disks perpendicular to the beam axis.

The first layer of the pixel detector with highest granularity, so-called **B-layer**, is very important for an excellent vertexing.

Typically 3 pixel layers and 8 SCT layers are crossed by a good quality track belonging to a charged particle.

A large number of hits, typically 36 per track, is measured with straw tubes of the **Transition Radiation Tracker (TRT)** which covers the η region up to $|\eta| < 2.0$ and creates the outermost part of the tracking detector.

The TRT detector enables also the **electron** vs. **pion** identification through the detection of transition radiation photons in the xenon-based gas mixture of its straw tubes.

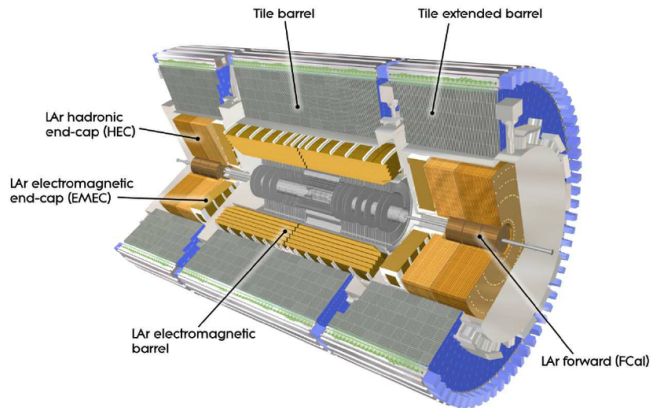
<https://atlas.cern/discover/detector/inner-detector>

Calorimeters

The ATLAS calorimetry system consists of different types of sampling calorimeters covering the total pseudorapidity range $|\eta| < 4.9$.

The fine granularity of the electromagnetic calorimeter in the region matched to the inner detector is necessary for precision measurements of **electrons** and **photons**.

The hadronic calorimeters are dedicated for the **jet reconstruction** and **missing transverse energy measurement** for which a coarser granularity is sufficient.



The electromagnetic (EM) system consists of two parts

1. The **presampler detector** is located in front of the EM calorimeter in the region $|\eta| < 1.8$. It is developed to correct for the energy lost in the material before the calorimeter. It consists of an active **liquid argon (LAr) layer** of thickness 1.1 cm in the barrel and 0.5 cm in the end-cap.
2. The **EM calorimeter** with the liquid argon LAr as an active material has a typical structure of an accordion-geometry with kapton electrodes and lead absorber plates. The calorimeter is symmetric in the azimuthal angle without any azimuthal cracks. The calorimeter is built of 3 longitudinal layers. Most of the EM shower energy for high E_T electrons and photons is collected in the middle layer which has a fine granularity of 0.025×0.025 in $\eta \times \phi$ space. The first layer, so-called **strip layer**, offers an excellent γ - π^0 discrimination. The last layer with coarser granularity collects the energy deposited in the tail of the very energetic EM showers. The EM calorimeter is divided into a **barrel region** ($|\eta| < 1.475$) and two **end-caps** ($1.375 < |\eta| < 3.2$).

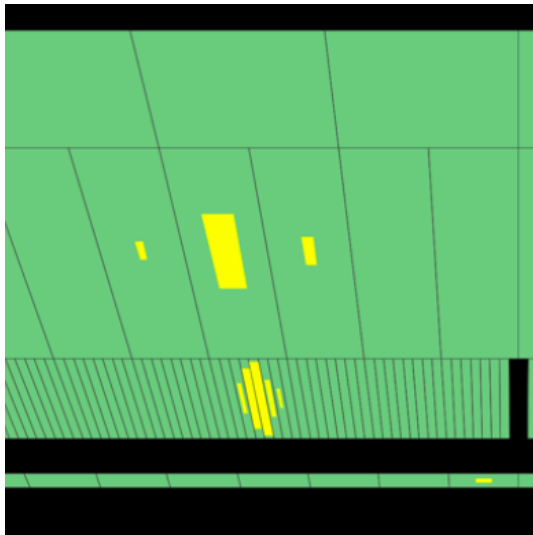


Figure 7: Photon, $E_T = 32$ GeV

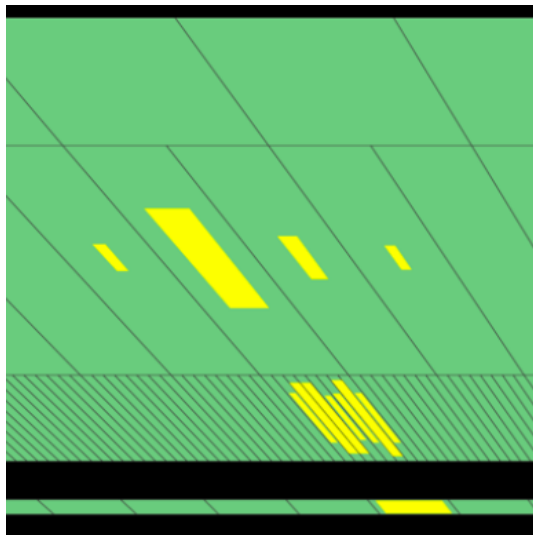


Figure 8: π^0 meson with BR = 98.823% to 2γ , $E_T = 21$ GeV

The Tile Calorimeter (TileCal) is a hadronic calorimeter covering the range $|\eta| < 1.7$ with steel used as an absorber and scintillating tiles as an active material.

The forward hadronic calorimeters use the LAr technology.

The Hadronic End-cap Calorimeter (HEC) covers pseudorapidity range $1.5 < |\eta| < 3.2$ using copper as the absorber.

Finally, the Forward Calorimeter (FCal) covers the most forward region up to $|\eta| < 4.9$. The FCal consists of three modules in each end-cap: The first module is made of copper and is optimised for electromagnetic measurements, the other two are made of tungsten and are used primarily for measurements of the hadronic showers.

→ Electromagnetic calorimeter resolution ($|\eta| < 3.2$): $\sigma_E/E = 10\%/\sqrt{E} \oplus 0.7\%$

→ Hadronic calorimeter resolution (jets):

▶ **Barrel and end-cap** ($|\eta| < 3.2$): $\sigma_E/E = 50\%/\sqrt{E} \oplus 3\%$

▶ **Forward region** ($3.1 < |\eta| < 4.9$): $\sigma_E/E = 100\%/\sqrt{E} \oplus 10\%$

<https://atlas.cern/discover/detector/calorimeter>

Muon spectrometer

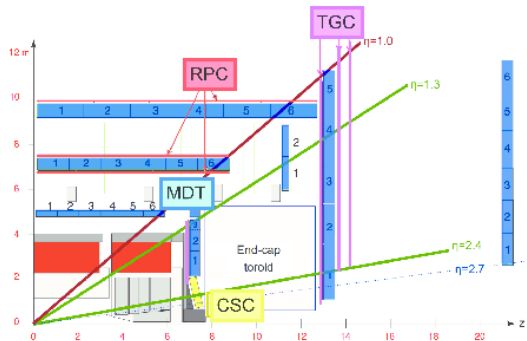
The muon spectrometer measures the deflection of the muon tracks in the magnetic field produced by large superconduction air-core toroid magnets (1 in the barrel and 2 in the end-caps) in the region $|\eta| < 2.7$.

The spectrometer chambers are arranged in 3 cylindrical layers around the beam axis while in the transition region and in the end-caps the chambers are installed in 3 planes perpendicular to the beam axis.

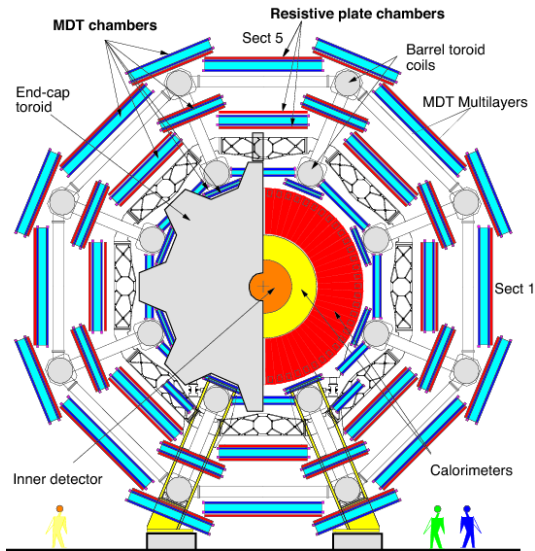
The **Monitored Drift Tubes (MDTs)** cover most of the pseudorapidity range of the muon system and provide a precision measurement of the muon tracks.

Cathode Strip Chambers (CSCs) with higher granularity are used in the large pseudorapidities ($2.0 < |\eta| < 2.7$). The CSCs are radiation resistant and can be used in a region with an increasing particle rate.

The muon trigger system covers the pseudorapidity range up to 2.4. **Resistive Plate Chambers (RPCs)** are used in the barrel and **Thin Gap Chambers (TGCs)** in the end-caps; used to measure the muon coordinate in the direction orthogonal to the precision-tracking chambers and also for triggering.



ATLAS



Magnets

The magnet system of ATLAS bends particles around the various layers of detector systems, making it easier to contain the tracks of particles. The main sections of the magnet system are: **Central Solenoid Magnet**, **Barrel Toroid** and **End-cap Toroids**.



Figure 9: Barrel Toroid

Arranged in an eight-fold azimuthal symmetry around the calorimeters - 4 T magnetic field on superconductor.

<https://atlas.cern/discover/detector/magnet-system>



Figure 10: End-cap toroid

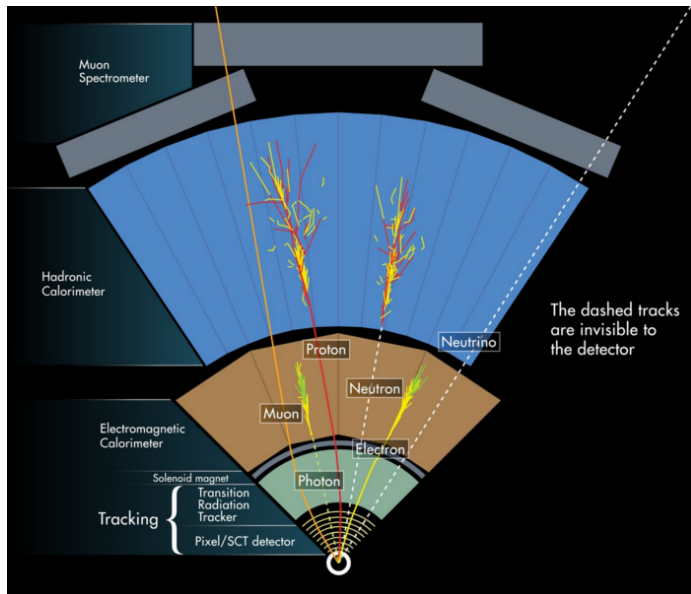
8 coils -4 T magnetic field on superconductor



Figure 11: Central Solenoid

Bends charged particles for momentum measurement - 2 T magnetic field

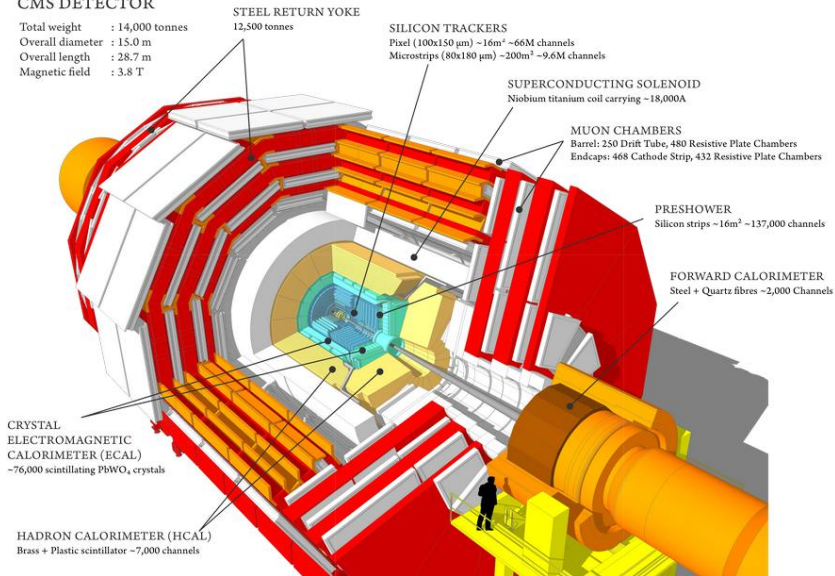
Overview of particle detection

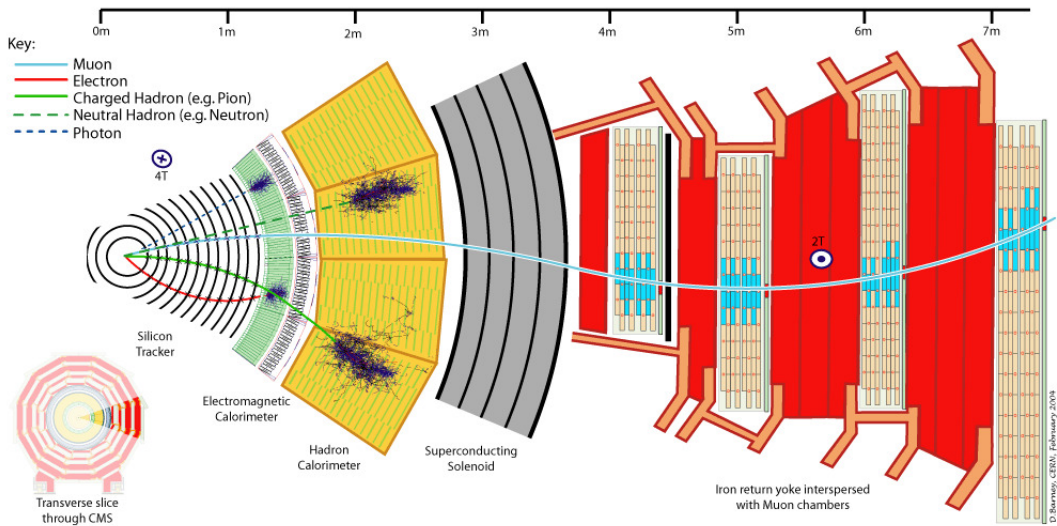


Compact Muon Solenoid

CMS DETECTOR

Total weight : 14,000 tonnes
Overall diameter : 15.0 m
Overall length : 28.7 m
Magnetic field : 3.8 T

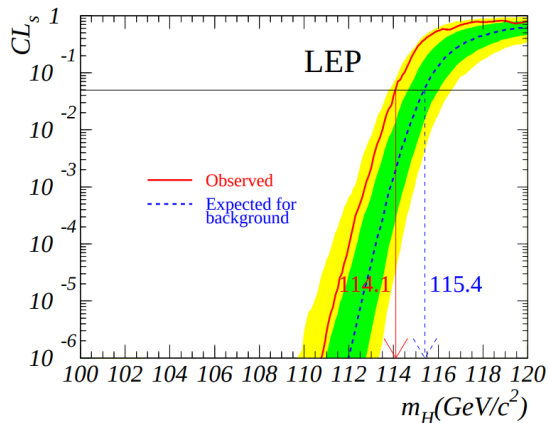




Searching for the Higgs boson

Prior to the turn-on of the Large Hadron Collider at CERN, the window for a Standard Model Higgs was relatively narrow.

The absence of a signal from the direct searches at LEP implied that $m_H > 114 \text{ GeV}$ 95% CL.



Confidence level CL_s for the signal+background hypothesis. **Solid line:** observation. **Dashed line:** median background expectation. The dark/light shaded bands around the median expected line correspond to the $\pm 1/\pm 2$ standard deviation spreads from a large number of background experiments (Ref. <https://arxiv.org/abs/hep-ex/0107029>).

At the same time, the limits on the size of the quantum loop corrections from the precision electroweak measurements at LEP and the Tevatron suggested that $m_H \lesssim 150$ GeV and that m_H was unlikely to be greater than 200 GeV.

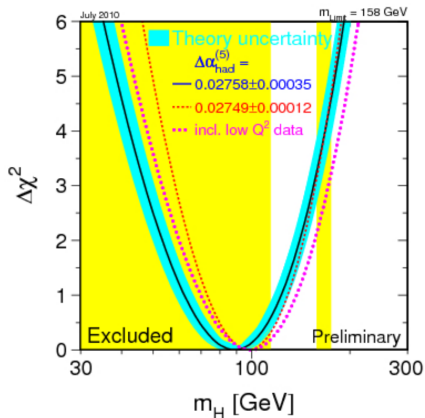


Figure 12: Indirect limits on Higgs mass driven by radiative corrections and from fits to electro-weak data.

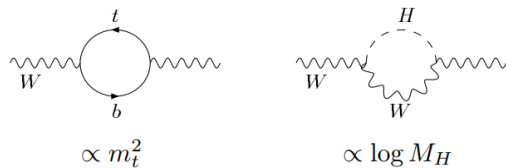


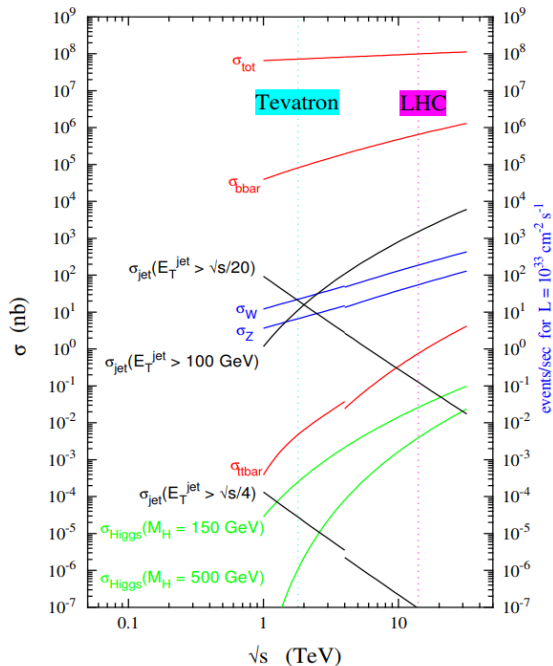
Figure 13: Quantum corrections to precision observables.

Searching Higgs at LHC

QCD background $\sigma_{b\bar{b}} \sim 10^9$ pb

Higgs signal $\sigma_{H+X} \sim 10$ pb

$\Rightarrow 3 \times 10^5$ Higgs bosons/year at
 $\int dt L = 30/\text{fb}$.

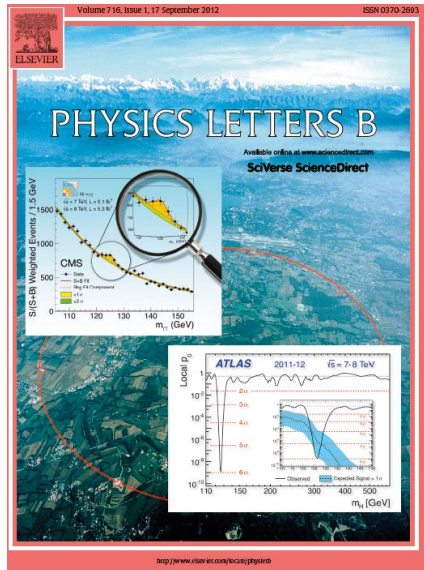


One of the main aims of the LHC was the discovery of the Higgs boson, assuming it existed.

The LHC is not only the highest-energy particle collider ever built, it is also the highest-luminosity proton-proton collider to date.

During 2010-2011 it operated at a center-of-mass energy of 7 TeV and during 2012-2017 at 8 TeV.

Compelling evidence of the discovery of a new particle compatible with the Standard Model Higgs boson was published by the ATLAS and CMS experiments in the Summer of 2012.



The Higgs boson can be produced at the LHC through a number of different processes, two of which are shown below:

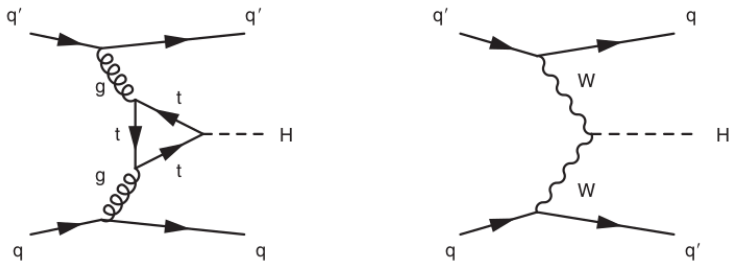


Figure 14: Two of the most important Feynman diagram for Higgs boson production in proton-proton collisions at the LHC. The [gluon-gluon fusion](#) process has a significantly higher cross section than the [vector-boson-fusion](#) process.

Because the Higgs boson couples preferentially to mass, the largest cross section at the LHC is through gluon-gluon fusion via a loop of virtual top quarks.

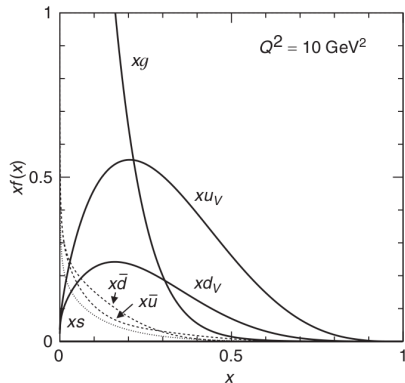
The cross section for this process can be written in terms of the underlying cross section for $gg \rightarrow H$ and the gluon Parton Distribution Functions (PDFs),

$$\sigma(pp \rightarrow hX) \sim \int_0^1 dx_1 \int_0^1 dx_2 g(x_1)g(x_2) \sigma(gg \rightarrow H) \quad (28)$$

where the Bjorken x is identified as the fraction of the momentum of the proton carried by the scattered parton.

The current understanding of the proton PDFs at $Q^2 = 10 \text{ GeV}^2$ as determined from the MRST fit to a wide range of experimental data.

The relatively small strange quark PDF $s(x)$ is shown. Taken from the Durham HepData project.



Consequently, the detailed knowledge of the PDFs for the proton is an essential component in the calculation of the expected Higgs boson production rate at the LHC.

Fortunately, the proton PDFs are well known and the related uncertainties on the various Higgs production cross sections are less than 10%.

Although the [ggH process has the largest cross section](#), from the experimental perspective the VBF process is also an important production mechanism.

This is because it results in more easily identifiable final states consisting of just the decay products of the Higgs boson and two forward-backward jets from the break-up of the colliding protons.

In contrast, the ggH n process is accompanied by QCD radiation from the colour field, making the identification of the Higgs boson final states more challenging.

Conclusions

The Higgs mechanism is an essential part of the Standard Model. It is based on a doublet of complex scalar fields with the Higgs potential $V(\phi) = \mu^2|\phi|^2 + \lambda|\phi|^4$ where $\mu^2 < 0$.

As a result, the vacuum state of the Universe is degenerate.

The spontaneous breaking of this symmetry, when combined with the underlying $SU(2)_L \times U(1)_Y$ gauge symmetry of the electroweak model, provides masses to the W and Z gauge bosons.

The interaction between the charged fermion fields and the non-zero expectation value of the Higgs field $v = 246$ GeV, provides a gauge-invariant mechanism for generating the masses of the Standard Model fermions.

One of the main goals of the Large Hadron Collider program is to discover the Higgs boson and measure its properties.